01

Prediction of emission spectra of red sprites using their miniature analogs and calculations of kinetic processes

© V.F. Tarasenko[1,2], A.S. Kirillov[2]

[1] Institute of High Current Electronics, Siberian Branch, Russian Academy of Sciences, Tomsk, Russia
[2] Polar Geophysical Institute, Russian Academy of Sciences, Apatity, Russia

e-mail: kirillov@pgia.ru

Received December 14, 2025
Revised February 16, 2026
Accepted March 01, 2026

It is proposed to obtain preliminary information on the emission spectra of red sprites at high resolution in various ranges using their laboratory analogs - plasma diffuse jets (PDJs). To substantiate predictions about the emission spectra of red sprites, the experimentally measured emission characteristics of PDJs were compared with the calculated data. In this case, a model describing kinetic processes involving electronically excited states of N_2 and N_2^+ in a mixture of N_2 and O_2 gases was used. A comparison was made of the theoretically calculated and experimentally measured ratios of the spectral emission densities of ten bands of the red and infrared ranges of the molecular nitrogen emission spectrum (first positive system) to the emission densities of the ultraviolet band of N_2 (second positive system) and the ultraviolet band of N_2^+ (first negative system) at medium pressures of 0.03−1 Torr.

Keywords: emission spectra, plasma diffuse jets, red sprites, theory and experiment.

DOI: 10.61011/0000000000

Introduction

To date, extensive information has been obtained about transient luminous events (TLE) [1,2], the radiation of which is caused by high-altitude discharges above thunderclouds. Thanks to research of discharges in the mesosphere and stratosphere from airplanes, satellites and the International Space Station, as well as in ground-based laboratories, information has been accumulated about the shape and nature of TLE [1–4]. Emission of red sprites is registered [5,6], a variety of blue jets [7,8], elves and halos [1–3]. However, the determination of the emission spectra of red sprites, which are the most studied, and other TLE is very difficult. These discharges are observed at altitudes of 40−100 km above sea level, mainly above thunderclouds that shield optical radiation. Accordingly, red sprites can be observed from the Earth at great distances from their place of occurrence or in the mountains. It is necessary to take into account the absorption of radiation in the Earth's atmosphere, which increases near its surface [9]. Measurements taken from airplanes, satellites, and the International Space Station make it possible to expand the information obtained, but they require high material costs. In addition, although red sprites appear above thunderclouds after positive lightning strikes reach the Earth's surface, the time and location of these discharges, as well as their shape, are unstable and vary from pulse to pulse [6].

Despite all these difficulties, work continues in which, in particular, the emission spectra of red sprites are studied. In the first papers in Ref. [10,11], it was shown that the red color of the sprites is due to the emission of bands of the first positive nitrogen system (1+):

$$N_2(B^3\Pi_g, \nu') \rightarrow N_2(A^3\Sigma_u^+, \nu'') + h\nu_{1+}. \quad (1)$$

Differences in the emission spectra at different heights and from different parts of red sprites were reported in Ref. [12–15]. Streamers propagating both down to the Earth's surface and upward, areas of bright glow (columnar glow), individual bright points (beads). However, the currently known data has been obtained with a relatively low spectral resolution, as well as in limited spectral ranges. Therefore, it is of practical interest to create a miniature analogue of red sprites, as well as other TLE, and to study their properties in the laboratory. Such studies began immediately after the discovery of the red sprites and are continuing at the present time. Most well-known works use a discharge having contact with metal electrodes [16]. Streamer discharges in the form of a jet are also modeled using a high-voltage electrode with a small radius of curvature [17,18]. Although there are no metal electrodes in atmospheric TLE. A dielectric film was used in Ref. [19] to form miniature red sprites without contact with a metal electrode, the surface of which was charged with a corona discharge. Then the chamber was vacuumed and at an air pressure corresponding to altitude above sea level of 51−68.3 km, two types of extended discharges occurred in a number of experiments. One of them was about 10 cm long and resembled a sprite in shape. The radiation spectra were measured at individual wavelengths in a wide range of pressures. Separate sections of bands of both 1+ and 2+ molecular nitrogen systems were recorded:

$$N_2(C^3\Pi_u, \nu') \rightarrow N_2(B^3\Pi_g, \nu'') + h\nu_{2+}, \quad (2)$$

as well as the Meinel (M) bands and the systems 1− of the molecular nitrogen ion:

$$N_2^+(A^2\Pi_u, \nu') \rightarrow N_2^+(X^2\Sigma_g^+, \nu'') + h\nu_M, \quad (3)$$

$$N_2^+(B^2\Sigma_u^+, \nu') \rightarrow N_2^+(X^2\Sigma_g^+, \nu'') + h\nu_{1-}. \quad (4)$$

However, the ratio of the spectral energy W between the individual bands was not determined, and data on the effect of pressure on W were not studied.

Significantly more information about the emission spectra was obtained in Ref. [20–24] using plasma diffuse jets (PDJ), miniature analogues of red sprites. Plasma diffuse jets were initiated by barrier discharge plasma due to positive and negative streamers. The study of PDJ at various pressures, high-voltage pulse generators, and discharge chamber designs made it possible to reproduce in the laboratory a number of properties of red sprites, primarily columnar (sprite front velocity, discharge color, and other characteristics). The emission spectra of red sprite analogues in the visible, ultraviolet, infrared and vacuum ultraviolet regions of the spectrum were recorded in Ref. [21,24]. However, in the obtained spectra, the ratios between the individual bands of nitrogen systems 1+ and 2+, as well as 1+ and 1− were not determined. In addition, the experimental data were not compared in Ref. [21,24] with the results of theoretical modeling of kinetic processes.

The purpose of this work is to show that using PDJ it is possible to predict the emission spectra of red sprites under various conditions, including from their individual parts. To prove this statement, a comparison of the experimental ratios of the spectral energy densities of radiation and the corresponding values obtained as a result of modeling was carried out. The calculations were carried out using a model of kinetic processes involving electronically excited molecules N_2 and N_2^+, created on the basis of a model of molecular nitrogen kinetics at altitudes of the high-latitude upper atmosphere during the precipitation of high-energy electrons [25,26].

Experimental unit and measurement procedures

The emission spectra of red sprite analogues were recorded using an installation similar to those described in Ref. [20–24]. Plasma diffuse jets, miniature analogues of red columnar sprites, were formed in quartz tubes during the initiating breakdown due to a capacitive discharge between 1 cm wide outer ring electrodes made of foil. A photograph of a discharge in a quartz tube obtained using a basic setup for studying the properties of PDJ is shown in Fig. 1.

The discharge was formed in a tube *2* made of quartz GE214 with an inner diameter of 5 cm and a wall thickness of 2.5 mm when connected to the outer ring electrodes *3, 4* of a high-voltage generator with an amplitude of voltage pulses in the absence of a breakdown $U \sim 10$ kV. The high-voltage and grounded electrodes, as well as their polarity, could be changed. The distance between the electrodes *3, 4* was 6 cm. The voltage decreased to ~ 7 kV in the pulse-periodic mode ($f = 21$ kHz), when the voltage pulse duration was at half-height $\sim 1.5\,\mu$s. The duration of the voltage front and voltagedrop were approximately the same and in the mode of formation of the PDJ were ~ 350 ns. It should be noted that after the end of the main voltage pulse, the discharge current continued in an oscillatory mode until about $5\,\mu$s. At the same time, sinusoidal voltage pulses with an amplitude of no more than 20,% of the maximum were observed in antiphase with the current. The radiation was output through the side wall of the quartz tube and could be detected at different distances from and between the electrodes.

The main attention in these experiments was paid to measuring the radiation spectra at a distance of 11 cm to the right of a high-voltage electrode *4* of negative polarity. The parameters of the PDJ radiation stabilized starting from a distance of ~ 6 cm from its right edge. At the same time, the electron temperature did not change significantly with distance from the high-voltage electrode at ~ 10 cm and was due to the spread of streamers (Fig. 10 in Ref. [22]).

The radiation spectra were recorded through the side wall of the quartz tube by an HR2000+ES spectrometer manufactured by OceanOptics Inc., which was equipped with a light guide. The sensitivity of the spectrometer and the transmission of the optical fiber in the range of 250−1000 nm were known. The spectral resolution of the optical system was no worse than 0.9 nm. The recording of the radiation spectra, as well as shooting the glow of the discharge plasma, was carried out in the dark. The quartz tube was filled with laboratory air with the relative humidity of ≈ 25 %.

Theoretical model

A model of kinetic processes involving the electronically excited states N_2 and N_2^+ in a mixture of gases N_2 and O_2 has been developed based on a model of molecular nitrogen kinetics at altitudes of the high-latitude upper atmosphere [25,26]. When calculating the excitation rates of various vibrational levels of five N_2 triplet states by electrons from discharge streamers, the following electronic excitation processes are taken into account:

$$e + N_2(X^1\Sigma_g^+, \nu = 0) \rightarrow$$

$$N_2(A^3\Sigma_u^+, B^3\Pi_g, W^3\Delta_u, B'^3\Sigma_u^-, C^3\Pi_u; \nu') + e. \quad (5)$$

In this case, the following vibrational levels of these triplet states are considered: $A^3\Sigma_u^+(\nu' = 0{-}29)$, $B^3\Pi_g(\nu' = 0{-}18)$, $W^3\Delta_u(\nu' = 0{-}21)$, $B'^3\Sigma_u^-(\nu' = 0{-}15)$, $C^3\Pi_u(\nu' = 0{-}4)$. Since radiative transitions occur between the considered states, in addition to spontaneous transitions (1) and (2) with the emission of bands 1+ and 2+,

it is also necessary to take into account the emission of the Wu-Benesch bands (transition $W^3\Delta_u, \nu' \leftrightarrow B^3\Pi_g, \nu''$) and afterglow bands (transition $B'^3\Sigma_u^+, \nu' \leftrightarrow B^3\Pi_g, \nu''$), as well as spontaneous transitions $A^3\Sigma_u^+, \nu' \rightarrow X^1\Sigma_g^+, \nu''$ (Vegard-Kaplan bands) [27].

In addition, the theoretical model includes the kinetics of triplet ($A^3\Sigma_u^+$, $B^3\Pi_g$, $W^3\Delta_u$, $B'^3\Sigma_u^-$, $C^3\Pi_u$) states N_2, taking into account inelastic collision processes:

$$N_2(Y, \upsilon') + N_2, O_2 \rightarrow N_2(B^3\Pi_g, \nu'') + N_2, O_2, \quad (6a)$$

$$N_2(B^3\Pi_g, \nu') + N_2, O_2 \rightarrow N_2(Y; \nu'') + N_2, O_2, \quad (6b)$$

where $Y = A^3\Sigma_u^+$, $W^3\Delta_u$, $B'^3\Sigma_u^-$ and

$$N_2(Y, \nu') + N_2(X^1\Sigma_g^+, \nu = 0) \rightarrow N_2(X^1\Sigma_g^+, \nu^* \geq 0) + N_2(Z, \nu''), \quad (7a)$$

$$N_2(Y, \nu') + O_2(X^3\Sigma_g^-, \nu = 0) \rightarrow N_2^{**} + O_2^{**}(O + O), \quad (7b)$$

where Y, Z = $A^3\Sigma_u^+$, $B^3\Pi_g$, $W^3\Delta_u$, $B'^3\Sigma_u^-$; N_2^{**}, O_2^{**} denote electronically or vibrationally excited molecules, and during the (7b) process, the repulsive state of O_2 may be excited with the dissociation of the molecule and the formation of two oxygen atoms. In contrast to the heights of the upper atmosphere, at the heights of the glow of sprites, the collisional lifetime of the molecule $N_2(C^3\Pi_u)$ becomes comparable to the radiative one, $\tau_C \sim 40$ ns, therefore, inelastic collisions $N_2(C^3\Pi_u)$ with molecules N_2 and O_2 must be taken into account. In the case of collisions with N_2, the quenching constants are taken into account according to [28], in case of collisions with O_2 — according to Ref. [29].

In addition to triplet states, model calculations take into account the processes of excitation of the doublet state $B^2\Sigma_u^+$ of the N_2^+ molecular nitrogen ion by electrons of the discharge streamers:

$$e + N_2(X^1\Sigma_g^+, \nu = 0) \rightarrow N_2^+(B^2\Sigma_u^+, \nu') + 2e. \quad (8)$$

For the ion $N_2^+(B^2\Sigma_u^+)$, inelastic collisions with molecules N_2 and O_2 are taken into account similarly to $N_2(C^3\Pi_u)$. In the case of collisions with N_2 and O_2, the quenching constants are taken into account according to Ref. [30]. This model allows calculating the luminescence intensity of the bands of the first (1+) and second (2+) positive systems of molecular nitrogen and the first negative (1−) system in a mixture of N_2 and O_2 gases during electrical discharges.

Let us calculate the rates of excitation of electronically excited states of molecular nitrogen by high-energy electrons during discharges by using the results of Ref. [31] on calculating the electron distribution function of a discharge. According to Ref. [31], with the pulse duration $\tau \sim 5\,\mu$s and the reduced electric field ~ 400 Td, the transient process of establishing the distribution function is quite fast and is on the order of 100 ns. At the same time, after the transient process, the average energy of the discharge electrons is about 8 eV for almost the entire pulse.

The excitation rates of various triplet states of molecular nitrogen (5) and the doublet state $B^2\Sigma_u^+$ of the ion N_2^+ (8) are determined by averaging the excitation cross sections taking into account the velocity distribution function $\langle\sigma(\nu)\nu\rangle$, where σ — is the excitation cross section according to Ref. [32] and ν — the velocity of electrons. For energies from 0 to 20 eV the distribution function according to Ref. [31], is close to the Maxwellian form. With a further increase in energy, it gradually deviates from the Maxwellian distribution. Since the maxima of the excitation cross-sections of N_2 triplet states by high-energy electrons are located in the region of 10−20 eV [32], the use of the Maxwell distribution in calculations practically does not distort the results of calculating the excitation rates of these N_2 molecular nitrogen triplet states.

For the $B^2\Sigma_u^+$ doublet state of the N_2^+ ion, the calculated excitation rates by high-energy electrons for the energy ranges 0−-40 eV and 0−1000 eV for the Maxwellian energy distribution of particles with average energy 4, 6, 8, 10 eV give minor discrepancies —less than 1, 5, 15, 28 %, respectively, which is associated with a sharp decrease in the values of the distribution function with increasing energy. Therefore, in our calculations we use the Maxwellian energy distribution of discharge electrons with average energies of 3, 4, 6, 10 eV. In addition, the calculations assumed that the electron concentration was of the order of the characteristic concentrations in the E region of the ionosphere: $N_e = 10^5$ cm^{-3}. However, the choice of this value does not affect the results of calculating the ratio of the spectral energy densities of the W radiation bands of the 1+, 2+, 1− systems of the N_2 molecule and the N_2^+ ion.

Results

The radiation spectra were recorded at different air pressures at a distance from the high-voltage electrode (Fig. 1). Two series of measurements were taken to compare the experimental and calculated data, each of which included six pressure values. In the first series, spectral energy densities of radiation were recorded at pressures of 1, 0.4, 0.1, 0.07, 0.05, 0.03 Torr, and in the second series spectral energy densities of radiation were recorded at pressures of 3, 1, 0.4, 0.2, 0.08, 0.04 Torr. In both series, the radiation spectra were recorded at a distance of 11 cm from the high-voltage electrode. As we have already noted, a relatively homogeneous PDJ was formed in this area (point S in Fig. 1) and further. Its diameter decreased as it moved away from the electrodes, but the color of the discharge remained.

The dependence of the radiation spectrum on the area of its measurement was studied earlier. The results obtained are presented in [22]. It was shown that in the area near the electrodes and between the electrodes, the ratio E/N (E —

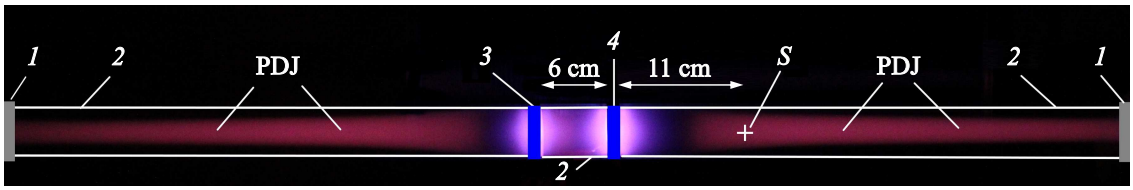


Figure 1. Photos of discharge radiation in a transparent tube with a negative polarity of the voltage pulses of the generator G2. *1* — caprolon end flanges, *2* — quartz tube, *3* — grounded electrode, *4* — high voltage electrode, PDJ — plasma diffuse PDJ jet, *S* — discharge region from which the emission spectra were recorded. Voltage pulse repetition rate 21 kHz, air pressure 0.4 Torr. The nozzle for pumping and venting gas is not shown.

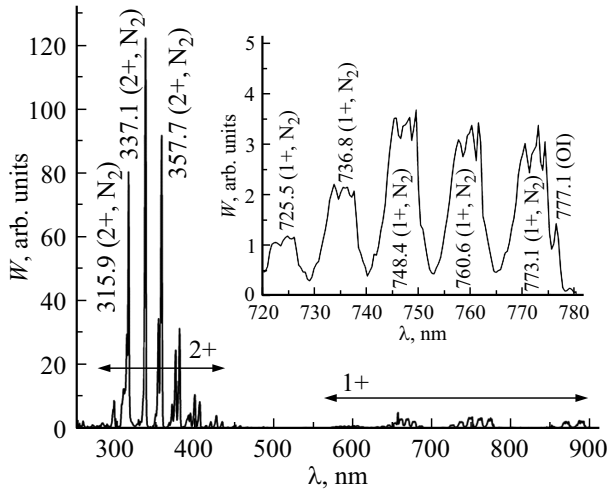


Figure 2. The emission spectrum of air at a pressure of 0.4 Torr from the range of *S* of the PDJ with a width of 1 cm, exposure 5 s, the inset shows in detail the radiation spectrum in the 720–780 nm region.

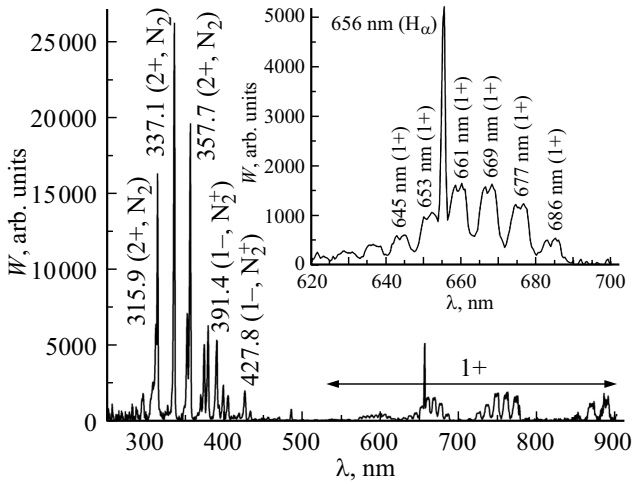


Figure 3. The emission spectrum of air at a pressure of 0.1 Torr from the range of *S* of the PDJ with a width of 1 cm, exposure 5 s, the inset shows in detail the radiation spectrum in the range of 620–700 nm.

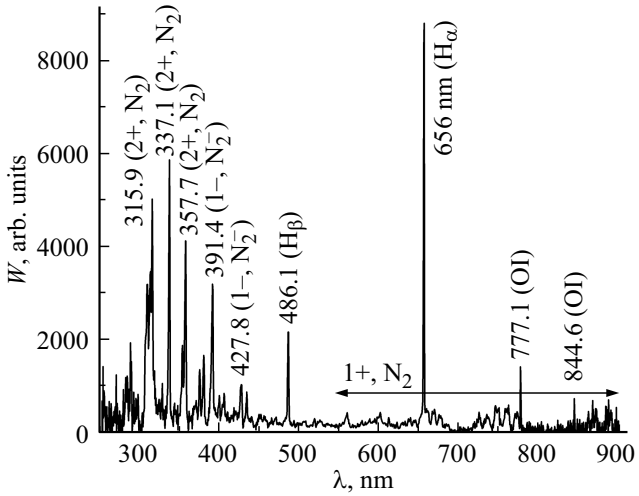


Figure 4. The emission spectrum of air at a pressure of 0.03 Torr from the area *S* of the LDS with a width of 1 cm, exposure 5 s.

electric field strength, N — concentration of gas particles) increases, which leads to an increase in the intensity of radiation in the UV region of the spectrum in the bands of 2+ and 1− nitrogen systems. In this case, the color of the discharge changes — a blue tint appears in it, and the color of the discharge turns white near the electrodes (the glow at the electrodes in Fig. 1). In the area of the PDJ propagation, the value of E/N decreased as it moved away from the electrodes, and the temperature of the electrons decreased accordingly. This affected the radiation spectrum and, consequently, the color of the discharge. The ratio between the spectral energy densities of the radiation bands 1+ and 2+ of molecular nitrogen in the PDJ did not change significantly when moving away from the electrodes.

A detailed comparison of the experimental data with the calculation results was given for the radiation spectra that were recorded in the first series. The data obtained in the second series at the same pressures and other equal conditions coincided with the data of the first series. It should be noted that the recording of a single radiation spectrum in the wavelength range 250–1000 nm was carried out in 105 000 pulses (exposure time 5 s). This determined the obtaining of the radiation spectrum in different areas under identical conditions and allowed for a small variation in the ratios of the spectral energy densities of the nitrogen bands 1+ and bands 2+ and 1−,

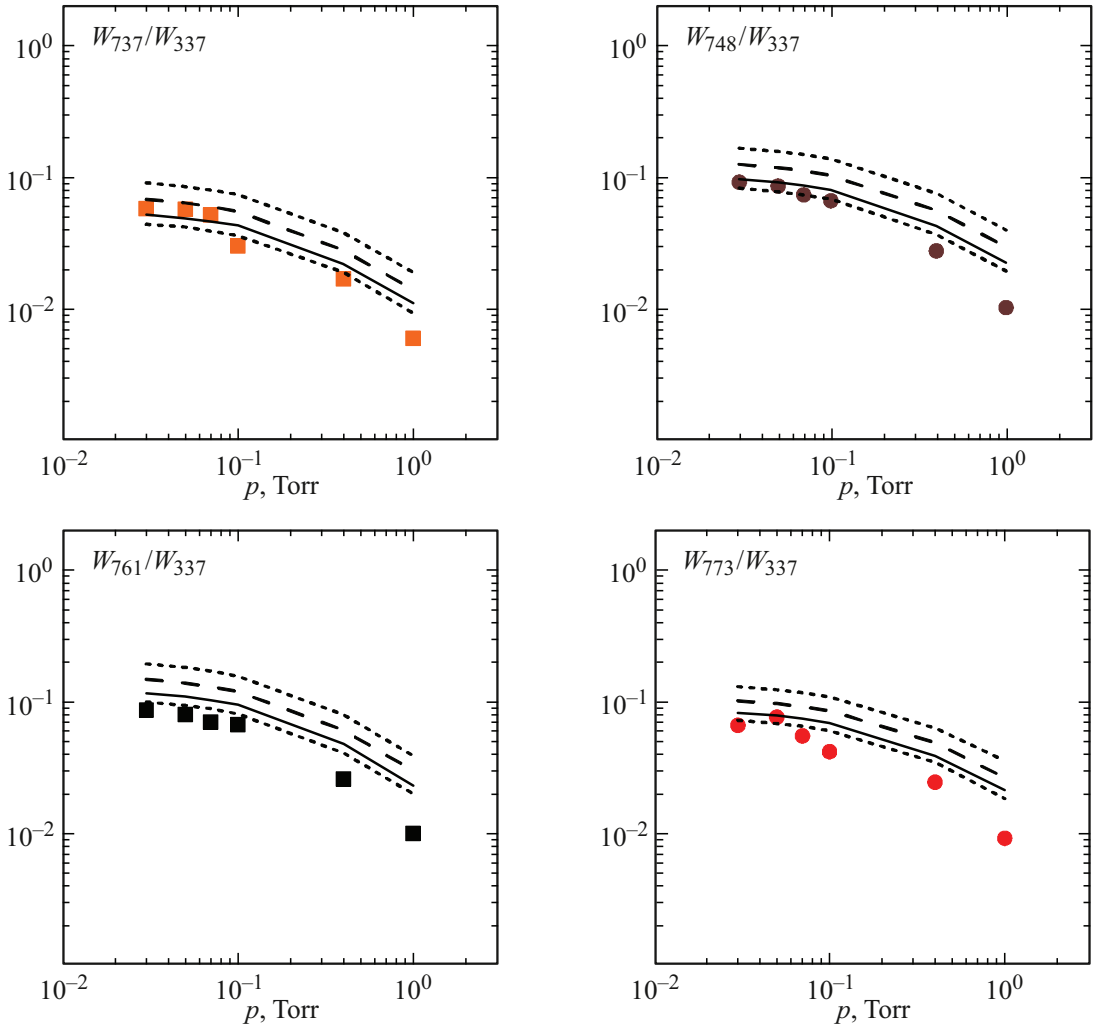


Figure 5. Comparison of experimentally measured values (squares, circles) of W_{1+}/W_{337} ($1+ = 737, 748, 761, 773$ nm) ratios with calculation results at average electron energies 3, 4, 6, 10 eV (respectively, upper dotted curves, dashed curves, solid curves, lower dotted curves).

which, when repeated measurements in each of the spectral regions, did not exceed 5%. Examples of radiation spectra for three different pressures are shown in Fig. 2–4.

Fig. 2 shows that the main contribution to the spectral energy density of W radiation is made by the bands of the 2+ and 1+ nitrogen molecule systems. It is known from Ref. [3,9] that radiation in the UV, visible, and IR regions of the spectrum was also recorded in the radiation of red sprites. The peak values of W for the ultraviolet bands 2+ were higher, but the visible red color of the PDJ is determined by the bands 1+. In addition, a line H_α of atomic hydrogen with a wavelength of 656.3 nm appears starting from an air pressure of 0.4 Torr at a relative humidity of ~ 25 %. Its appearance was due to the presence of water vapor in the air. With an increase in pressure (~ 1 Torr and more), the H_α line was not registered at constant relative humidity. The intensity of the line H_α decreased with a decrease in relative humidity at pressures of 0.4 Torr, and lower. The radiation spectrum did not contain this line in dry air. It should be noted that the appearance of the H_α line had no noticeable effect on the ratio between the W values of the 1+ and 2+ nitrogen bands.

When the air pressure in the quartz tube decreased by an order of magnitude, the voltage between the electrodes *3, 4* changed by no more than 20,%. This led to an increase in the reduced electric field strength and the appearance of bands of the first negative nitrogen ion system with wavelengths of 391.4 and 427.8 nm, as well as an increase in the intensity of the line H_α. These trends are illustrated in Fig. 3. Fig. 3 clearly shows that a decrease in air pressure led to the appearance of emission bands of the molecular nitrogen ion system 1−. The W values of the hydrogen line H_α and the ratio of the spectral energy densities of the bands W_{1+}/W_{2+} also increased. The specific values of the ratios W of the ten bands 1+ to W of the bands 2+ and 1−

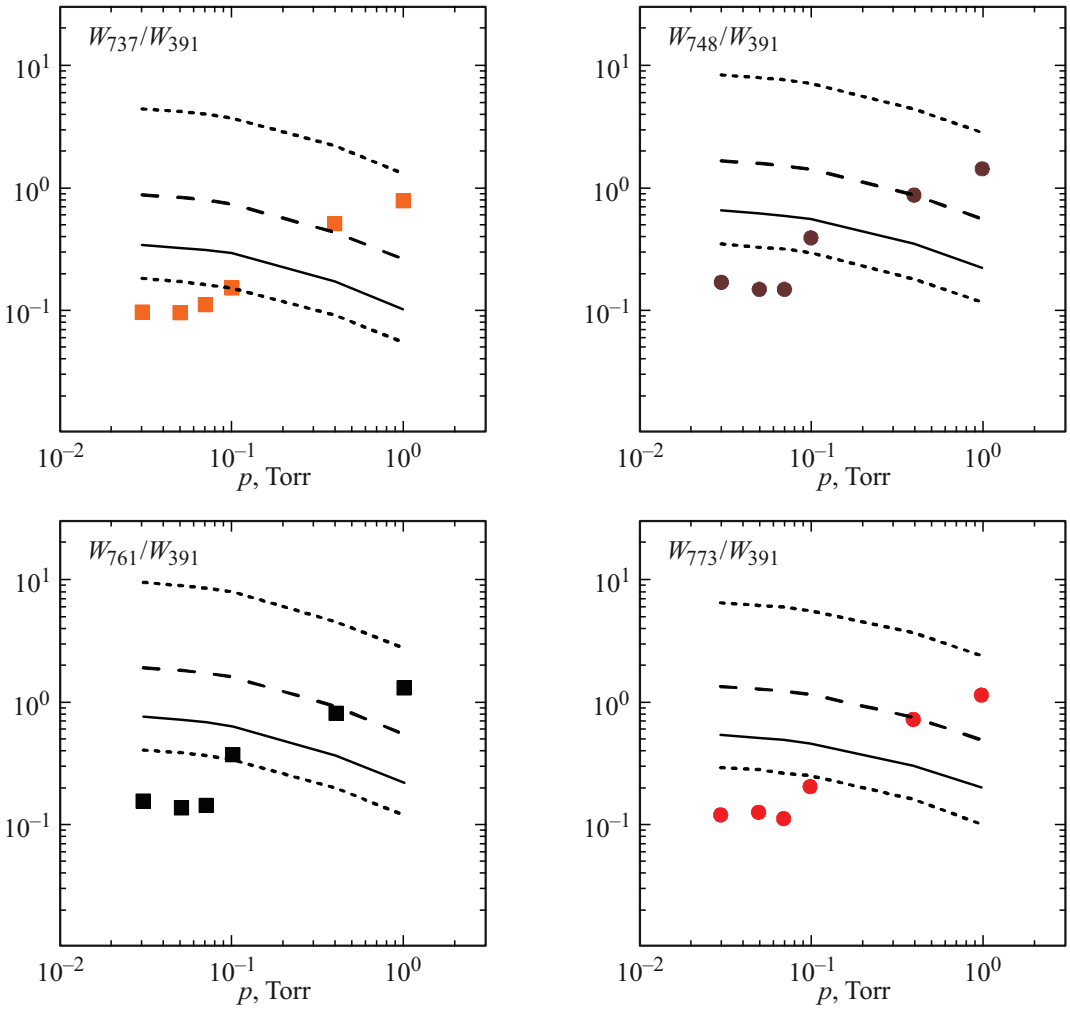


Figure 6. Comparison of experimentally measured values (squares, circles) of W_{1+}/W_{391} ($1+ = 737$, 748, 761, 773 nm) ratios with calculation results at average electron energies 4, 6, 8, 10 eV (respectively upper dotted curves, dashed curves, solid curves, lower dotted curves) for infrared bands of the first positive system.

will be given below when comparing the experimental and calculation results.

A further decrease in pressure leads to the continuation of these trends. The ratio of the spectral energy densities of the W_{1+} and W_{2+} bands increases. The radiation intensity of the hydrogen line H_α also increases and the line of the hydrogen atom H_β becomes noticeable. The radiation spectrum at an air pressure of 0.03 Torr, which corresponds to an altitude above sea level of 73 km, is shown in Fig. 4.

As the pressure decreased, the spectral energy density of the bands of the first negative system of the molecular nitrogen ion W_{1-} increased relative to the 2+ and 1+ bands. The intensity of radiation H_α and the continuum, which is clearly visible in the visible and ultraviolet regions of the spectrum at low pressures of air containing water vapor, also increased (Fig. 4). Previously, a similar continuum was recorded in Ref. [22] (Fig. 5, 6). Moreover, when registering the continuum at low pressures, the discharge color turned white (Fig. 2, *with* in Ref. [22]). We assume that the discharge color change is due to radiation at the junction $H_2(a^3\Sigma_g^+) \rightarrow H_2(b^3\Sigma_u^+)$ of hydrogen molecules, which is produced as a result of the dissociation of water vapor. The relative humidity of the air was about 25% in these experiments. We plan to study the radiation of the broadband continuum in our next work. In addition, atomic oxygen lines with wavelengths of 777.1 and 844.6nm appeared in the emission spectrum of air containing water vapor. Excited oxygen atoms can also appear as a result of the dissociation of water vapor.

Experimentally measured and theoretically calculated ratios of the spectral energy densities of the radiation bands 669 and 748 nm of the W_{1+} 1+ molecular nitrogen system to W_{2+} at a wavelength of 337 nm were compared in Ref. [33]. Similarly, the ratio W_{1+}/W_{2+} ratio for (1+)-bands 661, 669, 748, 761 nm and (2+)-bands 316, 337 nm was presented in Ref. [34].

The ratios of the spectral energy densities of the radiation of 1+ bands of W_{1+} molecular nitrogen at wavelengths 645,

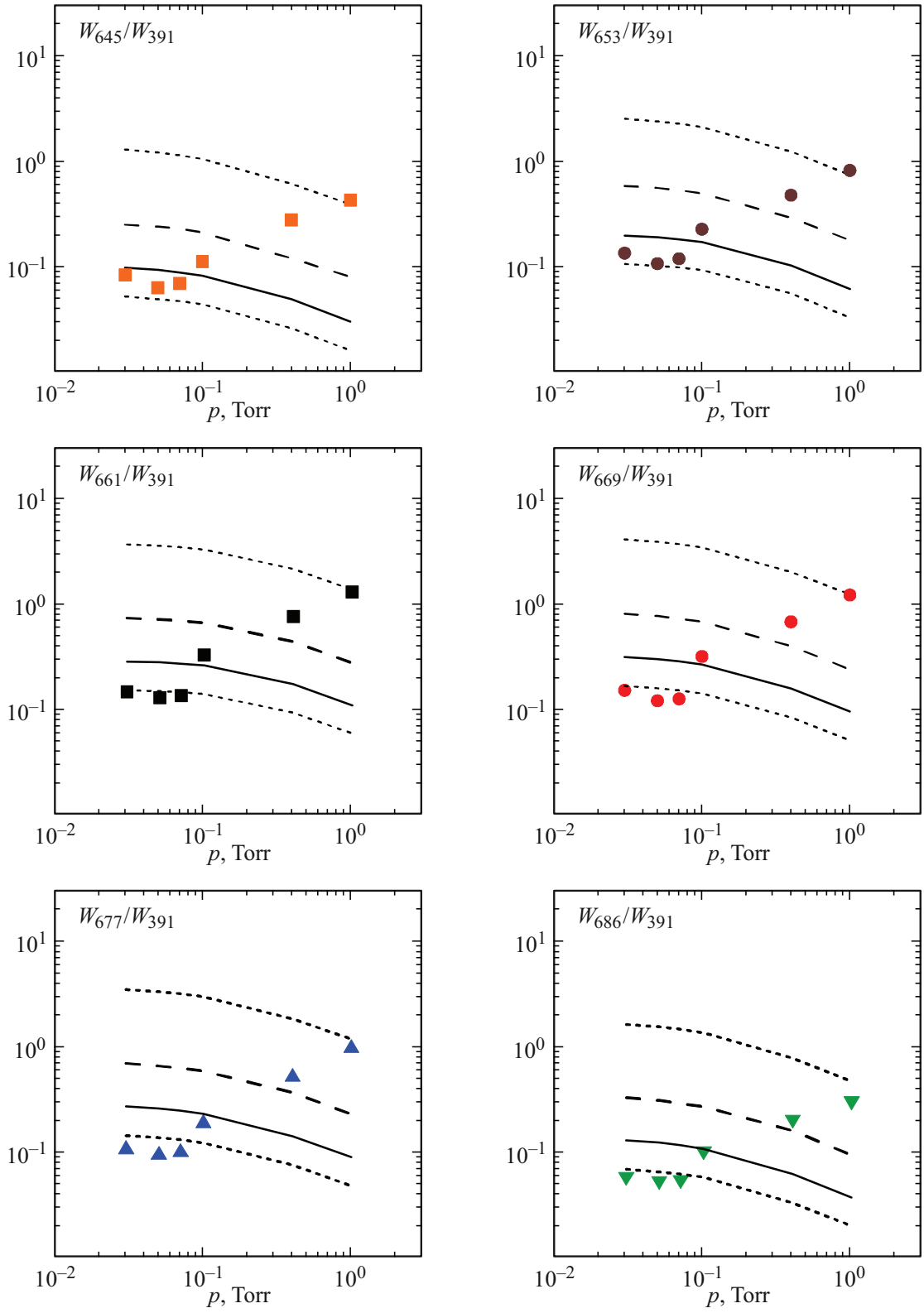


Figure 7. Comparison of experimentally measured values (squares, circles, triangles) of W_{1+}/W_{391} ($1+ = 645, 653, 661, 669, 677, 686$ nm) with the results of calculations at average electron energies 4, 6, 8, 10 eV (respectively upper dotted curves, dashed curves, solid curves, lower dotted curves) for the red bands of the first positive system.

653, 661, 669, 677, 686, 737, 748, 761, 773 nm to W_{2+} at a wavelength of 337 nm and to W_{1-} at a wavelength of 391 nm were determined in this study using the obtained N_2 radiation spectra. These ratios were also calculated using the theoretical model described above. Next, the experimentally measurements and theoretically calculated ratios of W_{1+}/W_{2+} and W_{1+}/W_{1-} were compared for the pressure range under consideration. The results of such a comparison for W_{1+}/W_{2+} are shown in Fig. 5, the results of such a comparison for W_{1+}/W_{1-} are shown in Fig. 6 and 7. Calculations were performed for the values of the average electron energies in the discharge plasma 3, 4, 6, 8, 10 eV.

Discussion of the received data

The use of the installation shown in Fig. 1 and other similar installations [20–24] made it possible to register radiation spectra from different sections of the PDJ, as well as to change the excitation conditions by using generators with different parameters and varying the design of the electrodes. By changing the excitation conditions, it was possible to create analogues of columnar red sprites formed by positive streamers [20], dots (beads) in them [23], separate areas of carrot red sprites with negative streamers [35] and columnar glow areas [36]. In addition, as can be seen from Fig. 5, there is a good agreement between the results of experimental studies of the spectral characteristics of air radiation at altitudes of red sprites. The measured and calculated ratios of the spectral energy densities of the 1+ bands of molecular nitrogen to the 2+ band coincide well at the electron temperature of $\sim 5-10$ eV. This temperature in the PDJ was also obtained by measuring the ratio of spectral energy densities for the 1− band with a wavelength of 391 nm to the 2+ band with a wavelength of 394 nm [22]. It can be assumed that the radiation spectra recorded for analogues of red sprites in Ref. [21,24] and our other publications make it possible to predict the radiation spectra in various regions of red sprites and their changes with varying conditions for the formation of altitude ranges.

In addition, according to experimental measurementsand theoretical calculations, a decrease in the W_{1+}/W_{2+} ratio is observed with increasing pressure. This is due to the fact that inelastic molecular collisions of (6b) and (7b) with an increase in the density of the medium lead to a significant decrease in populations of various vibrational levels of the state $B^3\Pi_g$ and, accordingly, to a decrease in the luminescence intensities of bands of 1+ molecular nitrogen N_2 caused by spontaneous radiative transitions from these vibrational levels.

The good agreement between the experimental and calculated data in Fig. 5 with a change in air pressure is due to the similarity of the dependence of the excitation cross sections of the $B^3\Pi_g$ and $C^3\Pi_u$ states on the electron energy. This eliminated the effect of air pressure on the electron temperature and led to a coincidence of the calculated and experimental values W_{1+}/W_{337}.

Fig. 6 and 7 show that as the pressure increases, the average temperature of the electrons in the experiment decreases. This leads to a consistent increase in the W_{1+}/W_{391} ratio with an increase in pressure above 0.07 Torr. The difference in the dependences of the W_{1+}/W_{391} and W_{1+}/W_{337} ratios in experiments and calculations is determined by the difference in the dependences of the excitation cross sections of the $B^2\Sigma_u^+$ and $C^3\Pi_u$ states on the electron energy. The temperature of the electrons was recorded during the calculations and the change in air pressure did not affect it.

Conclusion

Thus, a comparison of the theoretically calculated and experimentally measured ratios of the spectral radiation densities W_{1+}/W_{2+} and W_{1+}/W_{1-} for 10 bands of the N_2 1+ molecular nitrogen system to the 337 nm band of the 2+ molecular nitrogen system and to the 391 nm band of the 1− molecular nitrogen ion system at air pressures 0.03−1 Torr shows their compliance. Based on these data, it is assumed that the emission spectra of PDJ, which are analogues of red sprites, can be used to predict the emission characteristics of discharges at altitudes of 40−100 km and areas of red sprites with different properties. It has been established that inelastic molecular collisions with an increase in the density of the medium lead to a significant decrease in populations of various vibrational levels of the state $B^3\Pi_g$ and a decrease in the luminescence intensities of the bands 1+ N_2. It is shown that the considered ratios strongly depend on pressure and can be used to estimate the temperature of electrons in an exciting discharge. The information obtained at high spectral resolution and over a wide range of air pressures on the emission spectra of laboratory analogues of red sprites can be used in the study of physical processes in laboratory discharges and TLE.

Acknowledgments

The authors would like to thank N.P. Vinogradov, E.H. Baksht and V.A. Kirillov for their help in carrying out the work.

Funding

This study was supported by the Russian Science Foundation through grant No.25-22-00158.

References

[1] V.P. Pasko. J. Geophys. Res., **115** (6), A00E35 (2010). DOI: 10.1029/2009JA014860

[2] V.V. Surkov, M. Hayakawa. Surv. Geophys., **41** (5), 1101 (2020). DOI: 10.1007/s10712-020-09597-2

[3] F.J. Gordillo-Vázquez, F.J. Pérez-Invernón. Atmos. Res., **252**, 105432 (2021). DOI: 10.1016/j.atmosres.2020.105432
[4] V.A. Donchenko, M.V. Kabanov, B.V. Kaul', P.M. Nagorskij, I.V. Samohvalov. *Elektrooptícheskie yavleniya v atmosfere* (Izd-vo NTL, Tomsk, 2015) (in Russian).
[5] R.C. Franz, R.J. Nemzek, J.R. Winckler. Science, **249** (4964), 48 (1990). DOI: 10.1126/science.249.4964.48
[6] H.C. Stenbaek-Nielsen, R. Haaland, M.G. McHarg, B.A. Hensley, T. Kanmae. J. Geophys. Res., **115** (3), A00E12 (2010). DOI: 10.1029/2009JA014543
[7] E.V. Mishin, G.M. Milikh. Space Sci. Rev., **137** (1), 473 (2008). DOI: 10.1007/s11214-008-9346-z
[8] S. Soula, O.A. van Der Velde, J. Montanya, P. Huet, C. Barthe, J. Bór. J. Geophys. Res.: Atmos., **116** (D19), D19103 (2011). DOI: 10.1029/2010JD015581
[9] H.C. Stenbaek-Nielsen, M.G. McHarg, T. Kanmae, D.D. Sentman. Geophys. Res. Lett., **34** (11), L11105 (2007). DOI: 10.1029/2007GL029881
[10] S.B. Mende, R.L. Rairden, G.R. Swenson, W.A. Lyons. Geophys. Res. Lett., **22** (19), 2633 (1995). DOI: 10.1029/95GL02827
[11] D.L. Hampton, M.J. Heavner, E.M. Wescott, D.D. Sentman. Geophys. Res. Lett., **23** (1), 89 (1996). DOI: 10.1029/95GL03587
[12] R.A. Armstrong, J.A. Shorter, M.J. Taylor, D.M. Suszcynsky, W.A. Lyons, L.S. Jeong. J. Atm. Sol. Terr. Phys., **60** (7–9), 787 (1998). DOI: 10.1016/S1364-6826(98)00026-1
[13] C.L. Siefring, J.S. Morrill, D.D. Sentman, M.J. Heavner. J. Geophys. Res., **115** (A10), A00E57 (2010). DOI: 10.1029/2009JA014862
[14] F.J. Gordillo-Vázquez, A. Luque, M. Simek. J. Geophys. Res., **117** (A5), A05329 (2012). DOI: 10.1029/2012JA017516
[15] H.C. Stenbaek-Nielsen, M.G. McHarg, R. Haaland, A. Luque. J. Geophys. Res.: Atmos., **125** (20), e2020JD033170 (2020). DOI: 10.1029/2020JD033170
[16] Y. Goto, Y. Ohba, K. Narita. J. Atmos. Electricity, **27** (2), 105 (2007). DOI: 10.1541/jae.27.105
[17] D.F. Opaits, M.N. Shneider, P.J. Howard, R.B. Miles, G.M. Milikh. Geophys. Res. Lett., **37** (14), L14801 (2010). DOI: 10.1029/2010GL043996
[18] A.A. Evtushenko, M.E. Gushchin, S.V. Korobkov, A.V. Strikovskiy, E.A. Mareev. Geomag. Aeron., **60** (3), 345 (2020). DOI: 10.1134/S0016793220030068.
[19] A. Robledo-Martinez, A. Garcia-Villarreal, H. Sobral. J. Geophys. Res.: Space Physics, **122** (1), 948 (2017). DOI: 10.1002/2016JA023519
[20] E.Kh. Baksht, N.P. Vinogradov, V.F. Tarasenko. Atmos. Ocean. Opt., **35** (S1), S159 (2022). DOI: 10.1134/S1024856023010025.
[21] B.F. Tarasenko, E.Kh. Baksht, N.P. Vinogradov, D.A. Sorokin. Opt. Spectr., **130** (12), 1499 (2022). DOI: 10.21883/EOS.2022.12.55234.4014-22.
[22] D.A. Sorokin, V.F. Tarasenko, E.Kh. Baksht, N.P. Vinogradov. Phys. Plasmas, **30** (8), 083515 (2023). DOI: 10.1063/5.0153509
[23] V.F. Tarasenko, N.P. Vinogradov, E.Kh. Baksht, D.A. Sorokin, D.S. Pechenitsin. Atmos. Ocean. Opt., **37** (4), 547 (2024). DOI: 10.1134/S1024856024700738.
[24] V.F. Tarasenko, A.N. Panchenko, E.H. Baksht, N.P. Vinogradov. Opt. i spektr., **133** (1), 5 (2025) (in Russian). DOI: 10.61011/OS.2025.01.59873.7284-24
[25] A.S. Kirillov, V.B. Belakhovsky. Geophys. Res. Lett., **46** (3), 7734 (2019). DOI: 10.1029/2019GL083135
[26] A.S. Kirillov, V.B. Belakhovsky. Geomag. Aeron., **60** (1), 90 (2020). DOI: 10.1134/S0016793220010077.
[27] F.R. Gilmore, R.R. Laher, P.J. Espy. J. Phys. Chem. Ref. Data, **21** (5), 1005 (1992). DOI: 10.1063/1.555910
[28] A.S. Kirillov. Chem. Phys. Lett., **715**, 263 (2019). DOI: 10.1016/j.cplett.2018.11.048
[29] S.V. Pancheshnyi, S.M. Starikovskaia, A.Yu. Starikovskii. Chem. Phys., **262** (2), 349 (2000). DOI: 10.1016/S0301-0104(00)00338-4
[30] S.V. Pancheshnyi, S.M. Starikovskaia, A.Yu. Starikovskii. Chem. Phys. Lett., **294** (6), 523 (1998). DOI: 10.1016/S0009-2614(98)00879-3
[31] F.J. Gordillo-Vazquez. J. Phys. D, **41** (23), 234016 (2008). DOI: 10.1088/0022-3727/41/23/234016
[32] Y. Itikawa. J. Phys. Chem. Ref. Data, **35** (1), 31 (2006). DOI: 10.1063/1.1937426
[33] A.S. Kirillov, V.F. Tarasenko, N.P. Vinogradov, V.A. Kirillov. Geom. i aeron., **65** (6),), 897 (2025) (in Russian). DOI: 10.7868/S3034502225060118
[34] V.F. Tarasenko, N.P. Vinogradov, E.H. Baksht, A.S. Kirillov, V.A. Kirillov. Opt. atm. i okeana, **38** (9), 768 (2025) (in Russian). DOI: 10.15372/AOO20250911
[35] E.K. Baksht, V.F. Tarasenko, N.P. Vinogradov. Tech. Phys. Lett., **51** (3) 83 (2025). DOI: 10.61011/TPL.2025.03.60728.20152
[36] V.F. Tarasenko, D.A. Sorokin, E.Kh. Baksht, N.P. Vinogradov, V.A. Panarin, V.S. Skakun. Plasma Physics Reports, **51** (7), 830 (2025). DOI: 10.1134/S1063780X25603311

Translated by A.Akhtyamov